

This is the accepted manuscript made available via CHORUS. The article has been published as:

## Lattice dynamics of $\text{BaFe}_{\{2\}}\text{X}_{\{3\}}$ ( $\text{X}=\text{S}, \text{Se}$ ) compounds

Z. V. Popović, M. Šćepanović, N. Lazarević, M. Opačić, M. M. Radonjić, D. Tanasković,  
Hechang Lei (✉), and C. Petrovic

Phys. Rev. B **91**, 064303 — Published 27 February 2015

DOI: [10.1103/PhysRevB.91.064303](https://doi.org/10.1103/PhysRevB.91.064303)

# Lattice dynamics of $\text{BaFe}_2\text{X}_3$ ( $\text{X}=\text{S}, \text{Se}$ ) compounds

Z. V. Popović, M. Šćepanović, N. Lazarević, and M. Opačić  
*Center for Solid State Physics and New Materials, Institute of Physics Belgrade,  
University of Belgrade, Pregrevica 118, 11080 Belgrade, Serbia*

M. M. Radonjić  
*Scientific Computing Laboratory, Institute of Physics Belgrade,  
University of Belgrade, Pregrevica 118, 11080 Belgrade, Serbia and  
Center for Electronic Correlations and Magnetism, Theoretical Physics III,  
Institute of Physics, University of Augsburg, D-86135 Augsburg, Germany*

D. Tanasković  
*Scientific Computing Laboratory, Institute of Physics Belgrade,  
University of Belgrade, Pregrevica 118, 11080 Belgrade, Serbia*

Hechang Lei<sup>§</sup> and C. Petrovic  
*Condensed Matter Physics and Materials Science Department,  
Brookhaven National Laboratory, Upton, New York 11973-5000, USA  
(Dated: December 31, 2014)*

We present the Raman scattering spectra of the  $\text{BaFe}_2\text{X}_3$  ( $\text{X}=\text{S}, \text{Se}$ ) compounds in a temperature range between 20 K and 400 K. Although the crystal structures of these two compounds are both orthorhombic and very similar, they are not isostructural. The unit cell of  $\text{BaFe}_2\text{S}_3$  ( $\text{BaFe}_2\text{Se}_3$ ) is base-centered  $Cmcm$  (primitive  $Pnma$ ) giving totally 18 (36) modes to be observed in the Raman scattering experiment. We have detected almost all Raman active modes, predicted by factor group analysis, which can be observed from the cleavage planes of these compounds. Assignment of the observed Raman modes of  $\text{BaFe}_2\text{S}(\text{Se})_3$  is supported by the lattice dynamics calculations. The antiferromagnetic long-range spin ordering in  $\text{BaFe}_2\text{Se}_3$  below  $T_N=255$  K leaves a fingerprint both in the  $A_{1g}$  and  $B_{3g}$  phonon mode linewidth and energy.

PACS numbers: 78.30.-j; 63.20.D-; 75.50.-y; 74.70.Xa

## I. INTRODUCTION

The iron-based compounds are one of the top research fields in the condensed matter physics<sup>1</sup>. These materials are not only superconducting<sup>2</sup> but also form low-dimensional magnetic structures – spin-chains, spin-ladders or spin-dimers,<sup>3</sup> similar as in the case of cuprates<sup>4</sup> or vanadates.<sup>5</sup> Properties of iron-based selenide superconductors and other low dimensional magnetic phases of iron-chalcogenides are recently reviewed in Ref. 6.

$\text{BaFe}_2\text{S}_3$  and  $\text{BaFe}_2\text{Se}_3$  belong to the family of the iron-based  $S=2$  two-leg spin-ladder compounds. The crystal structure of these materials can be described as alternate stacking of Fe-S(Se) layers and Ba cations along the crystallographic  $a$ -axis ( $b$ -axis). In the Fe-S(Se) plane, only one-dimensional (1D) double chains of edge-shared  $[\text{FeS}(\text{Se})]_4$  tetrahedra propagate along the  $a$ -axis ( $b$ -axis), as shown in Figure 1. Although the crystal structures of the  $\text{BaFe}_2\text{S}_3$  and  $\text{BaFe}_2\text{Se}_3$  are isomorphic, they are not isostructural.  $\text{BaFe}_2\text{S}_3$  crystalizes in a base-centered orthorhombic structure with  $Cmcm$  space group.<sup>7</sup> The unit cell of  $\text{BaFe}_2\text{Se}_3$  is also orthorhombic but primitive of the  $Pnma$  space group. The main crystal structure difference of these compounds is an alternation of the Fe-Fe distances in  $\text{BaFe}_2\text{Se}_3$  along the chain direction which does not exist in  $\text{BaFe}_2\text{S}_3$ , where all distances between

Fe atoms along the chain direction are the same, see Fig.1(b), and Fig.1(c). This difference probably leads to the diverse magnetic properties of these two compounds at low temperatures.

$\text{BaFe}_2\text{S}_3$  is quasi-one-dimensional semiconductor. The magnetic susceptibility of  $\text{BaFe}_2\text{S}_3$ , measured at 100 Oe, showed the divergence of the field-cooled susceptibility and zero-field-cooled susceptibility with the cusp at 25 K (freezing temperature)<sup>8</sup> indicating the presence of short-range magnetic correlations and spin-glass-like behavior below 25 K. On the basis of these observations Gönen *et al.*<sup>8</sup> proposed that each  $[\text{Fe}_2\text{S}_3]^{2-}$  -chain possess strong intrachain antiferromagnetic coupling of Fe ions that is mediated through the sulfide ions. The combination of antiferromagnetic coupling, additional crystal field splitting due to neighboring Fe atoms, and direct Fe-Fe interactions presumably give rise to  $S = 0$  ground states in this compound.<sup>8</sup>

$\text{BaFe}_2\text{Se}_3$  is an insulator down to the lowest measured temperature with a long-range antiferromagnetic (AFM) order with  $T_N$  around 255 K and short-range AFM order at higher temperatures.<sup>9–12</sup> It was shown that a dominant order involves  $2 \times 2$  blocks of ferromagnetically aligned four iron spins, whereas these blocks order antiferromagnetically, in the same manner as the block-AFM  $\sqrt{5} \times \sqrt{5}$  state of the iron-vacancy ordered  $\text{A}_2\text{Fe}_4\text{Se}_5$ .<sup>13–15</sup>

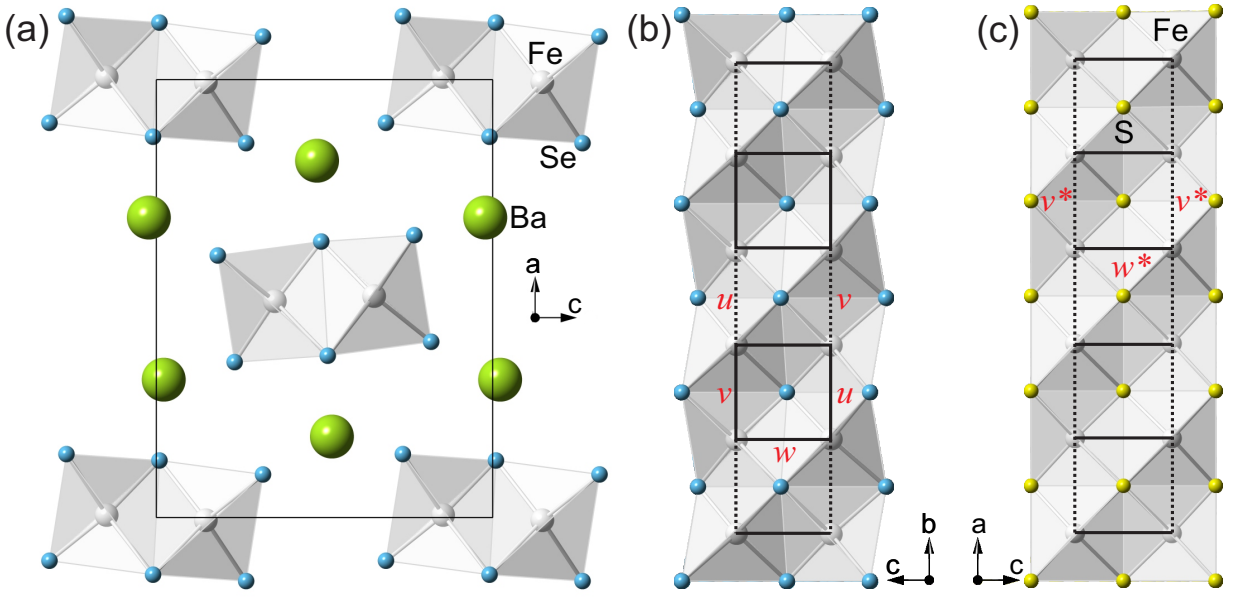


FIG. 1. (Color online) Schematic representation of the  $\text{BaFe}_2\text{X}_3$  ( $\text{X}=\text{S}, \text{Se}$ ) crystal structure. (a) Projection of the  $\text{BaFe}_2\text{X}_3$  crystal structure in the  $(ac)$  plane. (b) The double chain of Fe-Se tetrahedra connected via common edges along the  $b$ -axis. (c) The Fe-S double chain in the  $(010)$  projection.  $w, u, v$  represents Fe-Fe distances of ladder rungs ( $w=0.2697$  nm;  $w^*=0.2698$  nm) and legs ( $u=0.2688$  nm,  $v=0.2720$  nm;  $v^*=0.2643$  nm). Note that in the case of  $\text{BaFe}_2\text{S}_3$  the Fe atoms form an “ideal” ladder (all Fe-Fe distances along the ladder legs are equivalent, which is not a case in  $\text{BaFe}_2\text{Se}_3$ ).

To the best of our knowledge there are no data about the phonon properties of these compounds. In this paper we have measured polarized Raman scattering spectra of  $\text{BaFe}_2\text{X}_3$  ( $\text{X}=\text{S}, \text{Se}$ ) in the temperature range between 20 and 400 K. We have observed the Raman active optical phonons, which are assigned using polarized measurements and the lattice dynamical calculations. At temperatures below  $T_N=255$  K in  $\text{BaFe}_2\text{Se}_3$  the Raman modes shows an abrupt change of energy and linewidth due to the antiferromagnetic spin ordering.

## II. EXPERIMENT AND NUMERICAL METHOD

Single crystals of  $\text{BaFe}_2\text{X}_3$  ( $\text{X}=\text{S}, \text{Se}$ ) were grown using self-flux method with nominal composition  $\text{Ba}:\text{Fe}:\text{X}=1:2:3$ . Details were described in Ref. 16. Raman scattering measurements were performed on  $(110)$ (sulphide) [ $(100)$  (selenide)]-oriented samples in the backscattering micro-Raman configuration. Low temperature measurements were performed using KONTI CryoVac continuous flow cryostat coupled with JY T64000 and TriVista 557 Raman systems. The 514.5 nm line of an  $\text{Ar}^+/\text{Kr}^+$  mixed gas laser was used as excitation source. The Raman scattering measurements at higher temperatures were done using LINKAM THMS600 heating stage.

We calculated phonon energies of the nonmagnetic  $\text{BaFe}_2\text{S}(\text{Se})_3$  single crystals at the center of Brillouin zone. Calculations were performed within the theory of linear response using the density functional perturba-

tion theory (DFPT)<sup>17</sup> as implemented in QUANTUM ESPRESSO package.<sup>18</sup> In the first step, we obtained the electronic structure by applying the pseudopotentials based on the projected augmented waves method with the Perdew-Burke-Ernzerhof exchange-correlation functional and nonlinear core correction. Used energy cutoffs for the wave functions and electron densities were 80 (64) Ry and 960 (782) Ry for  $\text{BaFe}_2\text{S}(\text{Se})_3$ , respectively. We have carried out the calculation with experimental values of the  $\text{BaFe}_2\text{S}(\text{Se})_3$  unit cell parameters  $a=0.87835$  nm,  $b=1.1219$  nm,  $c=0.5286$  nm<sup>7</sup> ( $a=1.18834$  nm,  $b=0.54141$  nm,  $c=0.91409$  nm<sup>11</sup>), and the relaxed fractional coordinates, see Table I. Relaxation was applied to place atoms in their equilibrium positions in respect to used pseudopotentials (all forces acting on every atom were smaller than  $10^{-4}$  Ry/a.u.). The difference between experimental and relaxed coordinates is less than 3% for almost all atom coordinates, except for  $x$  direction of the Ba atoms in  $\text{BaFe}_2\text{Se}_3$ , which is 6%. Reduction of the  $x$  coordinate of Ba atoms by relaxation leads to an increase of the distance between the Ba layers. The Brillouin zone was sampled with  $8\times 8\times 8$  Monkhorst-Pack  $\mathbf{k}$ -space mesh. Calculated  $\Gamma$  point phonon energies of the  $\text{BaFe}_2\text{S}_3$  and  $\text{BaFe}_2\text{Se}_3$  are listed in Table II and Table IV, respectively.

The DFPT calculation of the phonon mode energies is performed assuming the paramagnetic solution and the comparison of energies is performed with the experimental results at room temperature. The paramagnetic density functional theory (DFT) solution is metallic, whereas  $\text{BaFe}_2\text{Se}_3$  is AFM insulator at low temperatures. Therefore, we have performed also the spin-polarized DFT calculations, assuming AFM ordering of  $2\times 2$  ferromagnetic

iron blocks.<sup>10–12</sup> We find the AFM solution and opening of the gap at the Fermi level in agreement with earlier DFT calculations by Saparov et al.<sup>10</sup> Accordingly, we attempted to calculate the phonon energies in the spin-polarized case. However, having now 48 atoms in the unit cell, this calculation turns out to be computationally too demanding. Furthermore, we do not believe that such a calculations would gives us in this case important new insights since the number of phonon modes becomes  $2 \times 72 - 1 = 143$  (one mode is degenerate), and it is not likely that small splitting of the modes could be compared with the experiments. Also, the phonon frequencies are not particularly sensitive on the precise form of the density of states near the Fermi level (or gap opening) if the overall spectral function remains similar. Therefore, we believe that the usage of the nonmagnetic DFT is reasonable method for identification of vibrational modes and comparison with the experimental data.

TABLE I. Experimental and relaxed [in square brackets] fractional coordinates of BaFe<sub>2</sub>S<sub>3</sub> (Ref. 7) and BaFe<sub>2</sub>Se<sub>3</sub> (Ref. 11) crystal structures.

Atom	Site	x	y	z
BaFe <sub>2</sub> S <sub>3</sub>				
Ba	(4c)	0.50 [0.50]	0.1859 [0.1817]	0.25 [0.25]
Fe	(8e)	0.3464 [0.3553]	0.50 [0.50]	0.00 [0.00]
S1	(4c)	0.50 [0.50]	0.6147 [0.6051]	0.25 [0.25]
S2	(8g)	0.2074 [0.2108]	0.3768 [0.3945]	0.25 [0.25]
BaFe <sub>2</sub> Se <sub>3</sub>				
Ba	(4c)	0.186 [0.175]	0.25 [0.25]	0.518 [0.513]
Fe	(8d)	0.493 [0.490]	0.002 [-0.001]	0.353 [0.358]
Se1	(4c)	0.355 [0.366]	0.25 [0.25]	0.233 [0.230]
Se2	(4c)	0.630 [0.613]	0.25 [0.25]	0.491 [0.485]
Se3	(4c)	0.402 [0.415]	0.25 [0.25]	0.818 [0.809]

### III. RESULTS AND DISCUSSION

#### A. BaFe<sub>2</sub>S<sub>3</sub>

The BaFe<sub>2</sub>S<sub>3</sub> crystal symmetry is orthorhombic, space group  $Cmcm$  and  $Z=4$ .<sup>7</sup> The site symmetries of atoms in  $Cmcm$  space group are  $C_{2v}^y$  (Ba, S1),  $C_2^x$  (Fe) and  $C_s^{xy}$  (S2). Factor group analysis yields:

$$(C_{2v}^y) : \Gamma = A_g + B_{1g} + B_{3g} + B_{1u} + B_{2u} + B_{3u},$$

$$(C_2^x) : \Gamma = A_g + 2B_{1g} + 2B_{2g} + B_{3g} + A_u + 2B_{1u} + 2B_{2u} + B_{3u}.$$

$$(C_s^{xy}) : \Gamma = 2A_g + 2B_{1g} + B_{2g} + B_{3g} + A_u + B_{1u} + 2B_{2u} + 2B_{3u}.$$

Summarizing these representations and subtracting the acoustic ( $B_{1u} + B_{2u} + B_{3u}$ ) and silent ( $2A_u$ ) modes, we

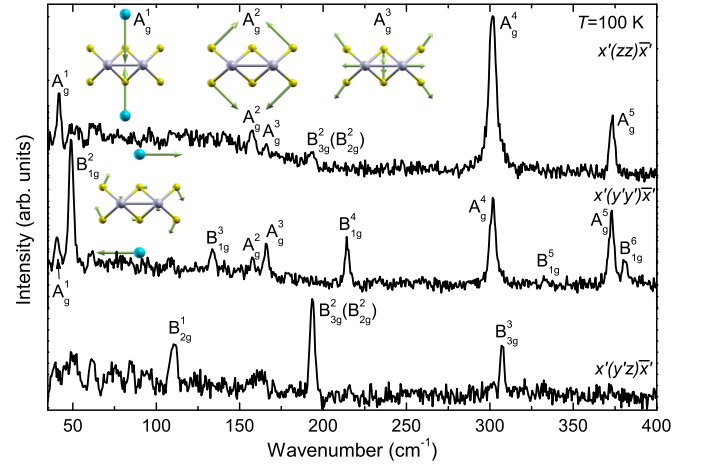


FIG. 2. (Color online) The polarized Raman scattering spectra of BaFe<sub>2</sub>S<sub>3</sub> single crystal measured at 100 K. Insets are the normal modes of the  $A_g^1$ ,  $A_g^2$ ,  $A_g^3$ , and  $B_{1g}^2$  vibrations.  $x'=[110]$ ,  $y'=[\bar{1}\bar{1}0]$ ,  $z=[001]$ .

obtained the following irreducible representations of BaFe<sub>2</sub>S<sub>3</sub> vibrational modes:

$$\Gamma_{BaFe_2S_3}^{optical} = 5A_g(xx, yy, zz) + 6B_{1g}(xy) + 3B_{2g}(xz) + 4B_{3g}(yz) + 4B_{1u}(E \parallel z) + 5B_{2u}(E \parallel y) + 4B_{3u}(E \parallel x)$$

Thus 18 Raman and 13 infrared active modes are expected to be observed in the BaFe<sub>2</sub>S<sub>3</sub> infrared and Raman spectra. Because our BaFe<sub>2</sub>S<sub>3</sub> single crystal samples have (110)-orientation, we were able to observe all symmetry modes in the Raman scattering experiment.

The polarized Raman spectra of BaFe<sub>2</sub>S<sub>3</sub>, measured from (110)-plane at 100 K are given in Figure 2. Five  $A_g$  symmetry modes at about 39, 157, 165, 301 and 373 cm<sup>-1</sup> (100 K) are clearly observed for the  $x'(zz)\bar{x}'$  polarization configuration ( $x'=[110]$ ,  $y'=[\bar{1}\bar{1}0]$ ,  $z=[001]$ ). For parallel polarization along the  $y'$ -axis the  $A_g$  and  $B_{1g}$  symmetry modes may be observed. By comparison ( $y'y'$ ) with ( $zz$ ) polarized spectrum we assigned the modes at 48, 133, 214, 332 and 381 cm<sup>-1</sup> as the  $B_{1g}$  ones. The intensity of the 332 cm<sup>-1</sup> mode is at a level of noise. Because of that assignment of this mode as  $B_{1g}^5$  one should be taken as tentative.

For the  $x'(y'z)\bar{x}'$  polarization configuration both the  $B_{2g}$  and the  $B_{3g}$  symmetry modes can be observed. Because we cannot distinguish the  $B_{2g}$  and  $B_{3g}$  by selection rules from the (110) plane the assignment of these modes was done with help of the lattice dynamics calculation, see Table II. Features between 40 and 100 cm<sup>-1</sup> come after subtracting of nitrogen vibration modes. Bump at about 160 cm<sup>-1</sup> is a leakage of  $A_g^2$  and  $A_g^3$  modes from parallel polarization.

The normal modes of some of  $A_g$ ,  $B_{1g}$  and  $B_{3g}$  vibrations, obtained by the lattice dynamics calculations, are given as insets in Figures 2 and 3. According to these representations the lowest energy  $A_g^1$  mode (39 cm<sup>-1</sup>) originates from the Ba atom vibrations along the  $y$ -axis, the  $A_g^2$  mode (157 cm<sup>-1</sup>) represents dominantly S atom

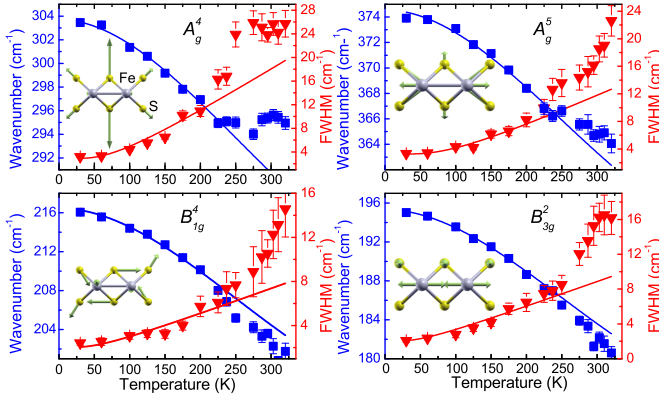


FIG. 3. (Color online) Experimental values (symbols) and calculated temperature dependence (solid lines) of the BaFe<sub>2</sub>S<sub>3</sub> Raman mode energies and broadenings. Insets represent the normal modes of the  $A_g^4$ ,  $A_g^5$ ,  $B_{1g}^4$ , and  $B_{3g}^2$  vibrations.

vibrations, which tend to elongate [Fe<sub>2</sub>S<sub>3</sub>]<sup>2-</sup>-chains along the  $y$ -axis. The  $A_g^3$  mode originates from both the sulphur and the iron atoms vibrations, which tend to stretch ladders along the  $x$ -axis. The  $A_g^4$  mode (Fig. 3) is sulphur atoms breathing vibrations, and the  $A_g^5$  symmetry mode represents the S and Fe atom vibrations with opposite tendency. The Fe atoms vibrate in opposite directions along the  $x$ -axis elongating the ladder, together with S atom vibrations, which tend to compress ladder structure.

Temperature dependence of the  $A_g^4$ ,  $A_g^5$ ,  $B_{1g}^4$  and  $B_{3g}^2$  mode energy and linewidth are given in Figure 3.

In general, temperature dependance of Raman mode energy can be described with:<sup>19</sup>

$$\omega(T) = \omega_0 + \Delta(T), \quad (1)$$

where  $\omega_0$  is temperature independent contribution to the energy of the phonon mode whereas  $\Delta(T)$  can be decomposed in:

$$\Delta(T) = \Delta^V + \Delta^A. \quad (2)$$

First term in Eq. (2) represents change of phonon energy due to the thermal expansion of the crystal lattice, and is given by:<sup>20</sup>

$$\Delta^V = -\omega_0 \gamma \frac{\Delta V(T)}{V_0}, \quad (3)$$

where  $\gamma$  is the Grüneisen parameter of a given mode.

Second term in Eq. (2) is contribution to the Raman mode energy from phonon-phonon scattering. By taking into account only three-phonon processes:

$$\Delta^A = -C \left( 1 + \frac{4\lambda_{\text{ph-ph}}}{e^{\hbar\omega_0/2k_B T} - 1} \right). \quad (4)$$

$C$  and  $\lambda_{\text{ph-ph}}$  are anharmonic constant and phonon-phonon interaction constant, respectively.

Temperature dependence of Raman mode linewidth is caused only by phonon anharmonicity:

$$\Gamma(T) = \Gamma_0 \left( 1 + \frac{2\lambda_{\text{ph-ph}}}{e^{\hbar\omega_0/2k_B T} - 1} \right), \quad (5)$$

where  $\Gamma_0$  is the anharmonic constant.

Parameter  $C$  is connected with  $\omega_0$  and  $\Gamma_0$  via relation:<sup>19</sup>

$$C = \frac{\Gamma_0^2}{2\omega_0}. \quad (6)$$

$\omega_0$  and  $\Gamma_0$  can be determined by extrapolation of the corresponding experimental data to 0 K. With these parameters known, we can fit the phonon mode linewidth, using Eq. (5), to obtain  $\lambda_{\text{ph-ph}}$ . Then, by determining parameter  $C$  via Eq. (6), Raman mode energy can be properly fitted, with  $\gamma$  as the only unknown parameter. Using data from Ref. 12 for the temperature change of the lattice constants of BaFe<sub>2</sub>Se<sub>3</sub> one can perform the corresponding analysis of the Raman mode energies temperature dependence.

The best fit parameters are collected in Table III. Because the  $\Gamma_0$  is very small in comparison to  $\omega_0$ , for all modes of both compounds (Table III), according to Eq.(6) the  $C$  anharmonic parameter becomes very small. Thus, contribution to the Raman mode energy from the phonon-phonon interaction can be neglected. In fact, a change of Raman mode energy with temperature is properly described only with the thermal expansion term  $\Delta^V$ , Eq.(3).

The most intriguing finding in Fig. 3 is a dramatic change of slope of the  $A_g^4$  mode linewidth (energy) temperature dependence at about 275 K. Because a hump in the inverse molar magnetic susceptibility<sup>8</sup>, as well as a change of slope of the electrical resistivity<sup>21</sup> temperature dependence are observed in BaFe<sub>2</sub>S<sub>3</sub> at about the same temperature we concluded that the deviation from anharmonic behaviour for  $A_g^4$  mode could be spin- and charge-related. In fact, many of iron-based spin-ladder materials have the 3D-antiferromagnetic phase transition at about 260 K. We believe that in the case of BaFe<sub>2</sub>S<sub>3</sub> the antiferromagnetic ordering of spins within the ladder legs changes from short-range to the long range state, without 3D antiferromagnetic spin ordering (the Néel state) of the whole crystal. This transition is followed with change of the electronic structure, which could explain the abrupt increase of the resistivity at this temperature<sup>21</sup>. A lack of the BaFe<sub>2</sub>S<sub>3</sub> low temperature crystallographic and transport properties measurements did not allow a more detailed study of a possible origin of the phonon energy and linewidth deviation from the anharmonic picture at about 275 K.

## B. BaFe<sub>2</sub>Se<sub>3</sub>

The BaFe<sub>2</sub>Se<sub>3</sub> unit cell consists of four formula units comprising of 24 atoms. The site symmetries of atoms in  $Pnma$  space group are  $C_s^{xz}$  (Ba, Se1, Se2, Se3) and  $C_1$  (Fe). Factor group analysis yields:

$$(C_s^{xz}) : \Gamma = 2A_g + 1B_{1g} + 2B_{2g} + 1B_{3g} + A_u + 2B_{1u} + 1B_{2u} + 2B_{3u},$$

TABLE II. Calculated and experimentally observed values of Raman active phonon mode energies (in  $\text{cm}^{-1}$ ) of  $\text{BaFe}_2\text{S}_3$  single crystal.

Symmetry	Calculation		Experiment		Activity
	relax.(unrelax.)		300 K	100 K	
$A_g^1$	42.3 (51.2)			39	(xx, yy, zz)
$A_g^2$	154.2 (156)			157	"
$A_g^3$	201.9 (167.4)		152	165	"
$A_g^4$	366.9 (294.8)		295	301	"
$A_g^5$	385.8 (307.1)		365	372	"
$B_{2g}^1$	107.8 (113.7)		107	109	(xz)
$B_{2g}^2$	224.1 (180.8)		181	193	"
$B_{2g}^3$	347.8 (283.6)				"
$B_{1g}^1$	16.7 (63)				(xy)
$B_{1g}^2$	55.1 (81.8)		44	48	"
$B_{1g}^3$	138.8 (153.1)		127	133	"
$B_{1g}^4$	243.5 (221.9)		203	214	"
$B_{1g}^5$	337.8 (241.6)			332(?)	"
$B_{1g}^6$	400.2 (330)		374	381	"
$B_{3g}^1$	55.1 (66.8)				(yz)
$B_{3g}^2$	201.1 (171.1)		181	193	"
$B_{3g}^3$	311.2 (308.7)		297	307	"
$B_{3g}^4$	369.3 (351.7)				"

TABLE III. The best fit parameters of  $\text{BaFe}_2\text{S}_3$  and  $\text{BaFe}_2\text{Se}_3$ .

Mode symmetry	$\omega_0$ ( $\text{cm}^{-1}$ )	$\gamma$	$\Gamma_0$ ( $\text{cm}^{-1}$ )	$\lambda$
$\text{BaFe}_2\text{S}_3$				
$A_g^4$	303.7(2)	3.7(2)	2.9(2)	2.8(5)
$A_g^5$	374.6(2)	2.6(2)	3.3(2)	1.9(3)
$B_{1g}^4$	216.5(2)	4.8(2)	2.0(3)	0.9(3)
$B_{3g}^2$	195.3(1)	5.2(2)	2.0(3)	1.0(1)
$\text{BaFe}_2\text{Se}_3$				
$A_g^8$	200.0(1)	1.6(2)	2.3(1)	0.4(1)
$A_g^9$	272.6(2)	1.4(1)	2.3(1)	0.6(1)
$A_g^{10}$	288.1(3)	1.8(2)	5.2(1)	0.3(1)
$A_g^{11}$	297.1(4)	1.4(2)	5.6(2)	0.4(1)

$$(C_1) : \Gamma = 3A_g + 3B_{1g} + 3B_{2g} + 3B_{3g} + 3B_{1u} + 3B_{2u} + 3B_{3u}.$$

Summarizing these representations and subtracting the acoustic ( $B_{1u}+B_{2u}+B_{3u}$ ) and silent ( $4A_u$ ) modes, we obtained the following irreducible representations of  $\text{BaFe}_2\text{Se}_3$  vibrational modes:

$$\Gamma_{\text{BaFe}_2\text{Se}_3}^{\text{optical}} = 11A_g + 7B_{1g} + 11B_{2g} + 7B_{3g} + 11B_{1u} + 7B_{2u} + 11B_{3u}$$

Thus 36 Raman and 29 infrared active modes are expected to be observed in the  $\text{BaFe}_2\text{Se}_3$  vibrational spectra. Because the  $\text{BaFe}_2\text{Se}_3$  single crystals have the (100)-orientation (the crystallographic  $a$ -axis is perpendicular to the plane of the single crystal), we were able to access only the  $A_g$  and the  $B_{3g}$  symmetry modes in the Raman scattering experiment.

The polarized Raman spectra of  $\text{BaFe}_2\text{Se}_3$ , measured from (100)-plane at room temperature and 20 K, for the parallel and crossed polarization configurations, are given in Figure 4. The spectra measured for parallel polarization configurations consist of the  $A_g$  symmetry modes.

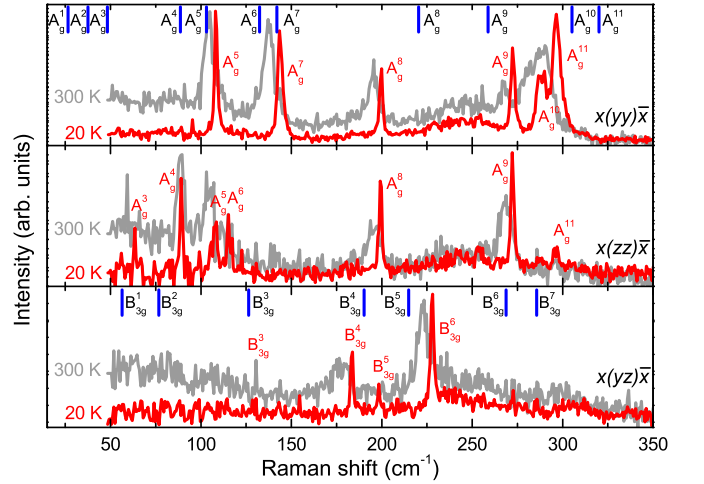


FIG. 4. (Color online) The  $x(yy)\bar{x}$ ,  $x(zz)\bar{x}$  and  $x(yz)\bar{x}$  polarized Raman scattering spectra of  $\text{BaFe}_2\text{Se}_3$  single crystals measured at room temperature and at 20 K. Vertical bars are calculated values of the  $A_g$  and the  $B_{3g}$  symmetry Raman active vibrations.

Six modes at about 108, 143.5, 200, 272, 288.7 and 296.5  $\text{cm}^{-1}$  (20 K) are clearly observed for the  $x(yy)\bar{x}$  polarization configuration and three additional modes are observed at about 63.4, 89, and 115  $\text{cm}^{-1}$  for the  $x(zz)\bar{x}$  polarization configuration. For the  $x(yz)\bar{x}$  polarization configuration three Raman active  $B_{3g}$  symmetry modes at 183.8, 198 and 228  $\text{cm}^{-1}$  (20 K) are observed. Vertical bars in Fig. 4 denote the calculated energies of the  $A_g$  and  $B_{3g}$  symmetry modes, which are in rather good agreement with experimentally observed ones. The results of the lattice dynamics calculations, together with the experimental data are summarized in Table IV.

According to the lattice dynamics calculations the lowest energy  $A_g^1$  mode is dominated by Ba atom vibrations along the  $\langle 101 \rangle$  directions, the  $A_g^2$  mode represents vibrations of Fe and Se atoms which tend to rotate  $[\text{Fe}_2\text{Se}_3]^{2-}$  chains around of the  $b$ -axis. The  $A_g^3$  mode



TABLE IV. Calculated and experimentally observed values of Raman active phonon mode energies (in  $\text{cm}^{-1}$ ) of  $\text{BaFe}_2\text{Se}_3$  single crystal.

Symmetry	Calc.	Experiment		Activity	Symmetry	Calc.	Experiment		Activity
		300 K	20 K				300 K	20 K	
$A_g^1$	26.5			(xx, yy, zz)	$B_{2g}^1$	25.8			(xz)
$A_g^2$	37.5			"	$B_{2g}^2$	48.0			"
$A_g^3$	48.3	59	63.4	"	$B_{2g}^3$	68.7			"
$A_g^4$	88.6	88	89	"	$B_{2g}^4$	88.8			"
$A_g^5$	103.0	104.3	108	"	$B_{2g}^5$	100.4			"
$A_g^6$	132.4	111	115	"	$B_{2g}^6$	138.2			"
$A_g^7$	142.0	137	143	"	$B_{2g}^7$	144.5			"
$A_g^8$	220.4	195.6	200	"	$B_{2g}^8$	212.9			"
$A_g^9$	258.8	267	272	"	$B_{2g}^9$	261.7			"
$A_g^{10}$	305.2	280	288.7	"	$B_{2g}^{10}$	303.9			"
$A_g^{11}$	320.2	290	296.5	"	$B_{2g}^{11}$	321.5			"
$B_{1g}^1$	56.4			(xy)	$B_{3g}^1$	56.4			(yz)
$B_{1g}^2$	72.8			"	$B_{3g}^2$	76.7			"
$B_{1g}^3$	126.2			"	$B_{3g}^3$	126.4			"
$B_{1g}^4$	191.4			"	$B_{3g}^4$	190.2	177	183.8	"
$B_{1g}^5$	210.5			"	$B_{3g}^5$	214.9		198	"
$B_{1g}^6$	267.1			"	$B_{3g}^6$	268.8	222.8	228	"
$B_{1g}^7$	285.2			"	$B_{3g}^7$	285.7			"

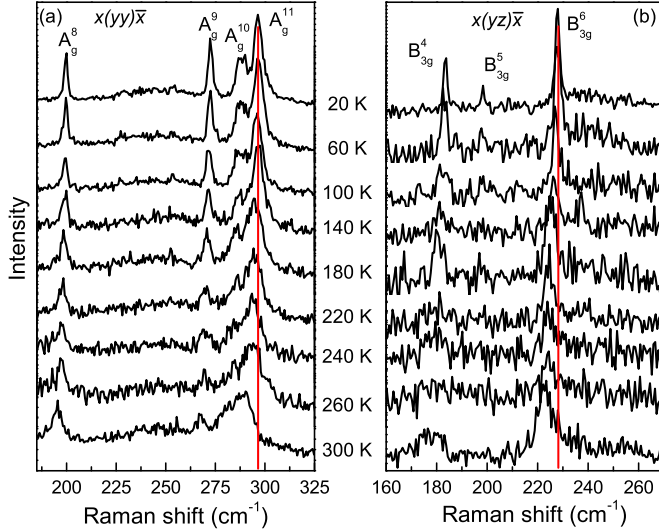


FIG. 5. The polarized Raman spectra of  $\text{BaFe}_2\text{Se}_3$  single crystals measured at various temperatures. (a)  $x(yy)\bar{x}$  polarization configuration; (b)  $x(yz)\bar{x}$  polarization configuration.

involves all atoms vibrations, which tend to stretch crystal structure along the  $\langle 101 \rangle$  directions, whereas the  $A_g^4$  mode originates from Se atom vibrations along the  $c$ -axis and the Fe atom vibrations along the  $\langle 101 \rangle$  directions. The  $A_g^5$  mode represents vibration of Fe and Se atoms, which lead to  $[\text{Fe}_2\text{Se}_3]^{2-}$  -chain compression along the  $c$ -axis. The  $A_g^6$  mode originates from Se and Fe atom vibrations which stretch  $[\text{Fe}_2\text{Se}_3]^{2-}$  -chains along the  $c$ -axis.

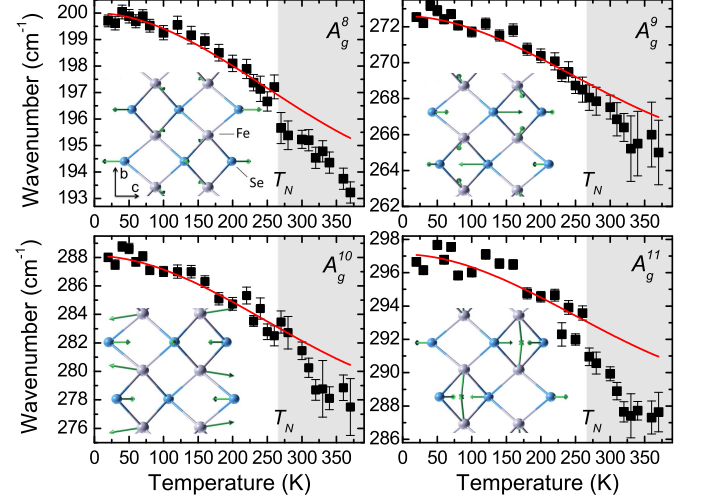


FIG. 6. (Color online) Experimental values (symbols) and calculated temperature dependence (solid lines) of  $\text{BaFe}_2\text{Se}_3$  Raman mode energies. The best fit parameters, for the temperature range below  $T_N$ , are given in Table III. Insets represent normal modes of the  $A_g^8$ ,  $A_g^9$ ,  $A_g^{10}$ , and  $A_g^{11}$  vibrations.

Finally, the  $A_g^7$  mode originates from Fe atom vibrations toward each other along the chain direction together with vibrations of the Se atoms along the  $c$ -axis. The normal coordinates of the  $A_g^8$ ,  $A_g^9$ ,  $A_g^{10}$ , and  $A_g^{11}$  modes are given as insets in Figure 6. As can be seen from Fig. 6 the  $A_g^8$  mode originates dominantly from Se atom stretching vibrations, whereas the  $A_g^9$ ,  $A_g^{10}$ , and  $A_g^{11}$  modes represent

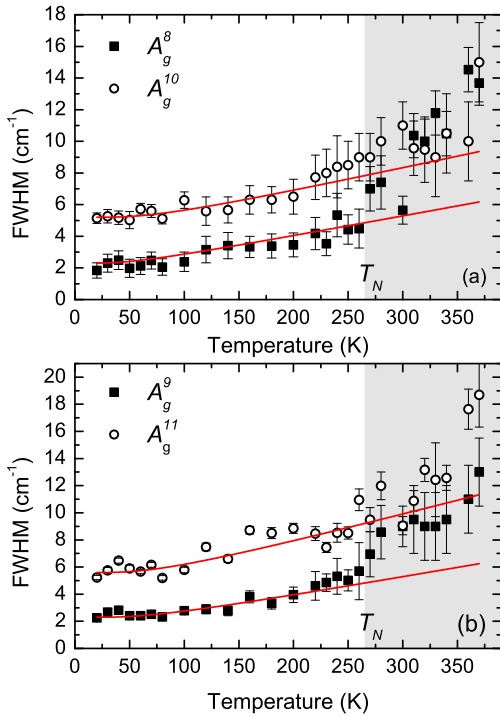


FIG. 7. Linewidth vs temperature dependence of (a) the  $A_g^8$  and  $A_g^{10}$  modes; (b)  $A_g^9$  and  $A_g^{11}$  modes of  $\text{BaFe}_2\text{Se}_3$ . Solid lines are calculated using Eq.(5). The best fit parameters for a temperature range below  $T_N$  are given in Table III.

vibrations of both the Se and Fe atoms. In fact, the  $A_g^9$  mode represents mostly Se atom vibrations along the  $c$ -axis, the  $A_g^{10}$  mode consists of Fe and Se vibrations along the  $c$ -axis, which tend to elongate ladder structure along the  $b$ -axis. Finally, the  $A_g^{11}$  mode represents the Fe atom vibrations toward each other along the chain axis together with Se atom vibrations perpendicular to the chain direction.

By lowering the temperature the lattice parameters of  $\text{BaFe}_2\text{Se}_3$  decrease continuously without the crystal symmetry change around the magnetic ordering temperature<sup>11,12</sup>  $T_N=255$  K. Consequently we should expect the Raman mode hardening, without any abrupt change. Contrary to the expectations the  $A_g$  and  $B_{3g}$  modes (see Figures 5, 6 and 7) sharply increase their energies below the phase transition temperature  $T_N$ , as it

is shown in details in the Figure 6. Because a significant local lattice distortion (Fe atom displacement along the  $b$ -axis is as large as approximately 0.001 nm)<sup>11,12</sup> exists, driven by the magnetic order, we concluded that spin-phonon (magnetoelastic) coupling is responsible for Raman mode energy and linewidth change in the antiferromagnetic phase. In fact, the existence of local displacements in the Fe atoms at  $T_N$  have a significant impact on the electronic structure due to rearrangement of electrons near the Fermi level<sup>11</sup> and consequently the change in the phonon energy and broadening. Raman mode linewidth change at about  $T_N$  is clearly observed as deviation from the usual anharmonicity temperature dependence (solid lines in Fig. 7) for all modes presented in Fig. 6.

#### IV. CONCLUSION

We have measured the polarized Raman scattering spectra of the  $\text{BaFe}_2\text{S}_3$  and  $\text{BaFe}_2\text{Se}_3$  single crystals in a temperature range between 20 K and 400 K. Almost all Raman-active modes predicted by factor-group analysis to be observed from the cleavage planes of  $\text{BaFe}_2\text{S}_3$  (110) and  $\text{BaFe}_2\text{Se}_3$  (100) single crystals, are experimentally detected and assigned. Energies of these modes are in rather good agreement with the lattice dynamics calculations. The  $\text{BaFe}_2\text{Se}_3$  Raman modes linewidth and energy, change substantially at temperatures below  $T_N=255$  K, where this compound becomes antiferromagnetically long-range ordered.

#### V. ACKNOWLEDGMENTS

This work was supported by the Serbian Ministry of Education, Science and Technological Development under Projects ON171032, ON171017 and III45018. Work at Brookhaven was supported by the Center for Emergent Superconductivity, an Energy Frontier Research Center funded by the US DOE, Office for Basic Energy Science (H.L. and C.P.). Numerical simulations were run on the AEGIS e-Infrastructure, supported in part by FP7 projects EGI-InSPIRE and PRACE-3IP.

<sup>§</sup>Present address: Department of Physics, Renmin University of China, 59 Zhongguancun Street, Haidian District, Beijing, 100872, China

<sup>1</sup> C. King and D. A. Pendlebury, Web of knowledge research fronts 2013, 100 Top-Ranked Specialties in the Sciences and Social Sciences, <http://sciencewatch.com/sites/sw/files/sw-article/media/research-fronts-2013.pdf>.

<sup>2</sup> Y. Kamihara, T. Watanabe, M. Hirano, and H. Hosono, J. Am. Chem. Soc. **130**, 3296 (2008).

<sup>3</sup> Z. V. Popović, M. Šćepanović, N. Lazarević, M. M. Radonjić, D. Tanasković, H. Lei, and C. Petrovic, Phys. Rev. B **89**, 014301 (2014).

<sup>4</sup> Z. V. Popović, M. J. Konstantinović, V. A. Ivanov, O. P. Khuong, R. Gajić, A. Vietkin, and V. V. Moshchalkov, Phys. Rev. B **62**, 4963 (2000).

<sup>5</sup> M. J. Konstantinović, Z. V. Popović, M. Isobe, and Y. Ueda, Phys. Rev. B **61**, 15185 (2000).

<sup>6</sup> E. Dagotto, Rev. Mod. Phys. **85**, 849 (2013).

<sup>7</sup> H. Hong and H. Steinfink, Journal of Solid State Chemistry **5**, 93 (1972).

<sup>8</sup> Z. S. Gönen, P. Fournier, V. Smolyaninova, R. Greene, F. M. Araujo-Moreira, and B. Eichhorn, Chemistry of



- Materials **12**, 3331 (2000).
- <sup>9</sup> H. Lei, H. Ryu, A. I. Frenkel, and C. Petrovic, Phys. Rev. B **84**, 214511 (2011).
  - <sup>10</sup> B. Saparov, S. Calder, B. Sipos, H. Cao, S. Chi, D. J. Singh, A. D. Christianson, M. D. Lumsden, and A. S. Sefat, Phys. Rev. B **84**, 245132 (2011).
  - <sup>11</sup> J. M. Caron, J. R. Neilson, D. C. Miller, A. Llobet, and T. M. McQueen, Phys. Rev. B **84**, 180409 (2011).
  - <sup>12</sup> Y. Nambu, K. Ohgushi, S. Suzuki, F. Du, M. Avdeev, Y. Uwatoko, K. Munakata, H. Fukazawa, S. Chi, Y. Ueda, and T. J. Sato, Phys. Rev. B **85**, 064413 (2012).
  - <sup>13</sup> F. Ye, S. Chi, W. Bao, X. F. Wang, J. J. Ying, X. H. Chen, H. D. Wang, C. H. Dong, and M. Fang, Phys. Rev. Lett. **107**, 137003 (2011).
  - <sup>14</sup> N. Lazarević, M. Abeykoon, P. W. Stephens, H. Lei, E. S. Bozin, C. Petrovic, and Z. V. Popović, Phys. Rev. B **86**, 054503 (2012).
  - <sup>15</sup> N. Lazarević, H. Lei, C. Petrovic, and Z. V. Popović, Phys. Rev. B **84**, 214305 (2011).
  - <sup>16</sup> H. Lei, H. Ryu, V. Ivanovski, J. B. Warren, A. I. Frenkel, B. Cekic, W.-G. Yin, and C. Petrovic, Phys. Rev. B **86**, 195133 (2012).
  - <sup>17</sup> S. Baroni, S. de Gironcoli, A. Dal Corso, and P. Giannozzi, Rev. Mod. Phys. **73**, 515 (2001).
  - <sup>18</sup> P. Giannozzi, S. Baroni, N. Bonini, M. Calandra, R. Car, C. Cavazzoni, D. Ceresoli, G. L. Chiarotti, M. Cococcioni, I. Dabo, A. D. Corso, S. de Gironcoli, S. Fabris, G. Fratesi, R. Gebauer, U. Gerstmann, C. Gougoussis, A. Kokalj, M. Lazzeri, L. Martin-Samos, N. Marzari, F. Mauri, R. Mazzarello, S. Paolini, A. Pasquarello, L. Paulatto, C. Sbraccia, S. Scandolo, G. Sciauzero, A. P. Seitsonen, A. Smogunov, P. Umari, and R. M. Wentzcovitch, Journal of Physics: Condensed Matter **21**, 395502 (2009).
  - <sup>19</sup> H.-M. Eiter, P. Jaschke, R. Hackl, A. Bauer, M. Gangl, and C. Pfleiderer, Phys. Rev. B **90**, 024411 (2014).
  - <sup>20</sup> V. Gnezdilov, Y. Pashkevich, P. Lemmens, A. Gusev, K. Lamonova, T. Shevtsova, I. Vitebskiy, O. Afanasiev, S. Gnatchenko, V. Tsurkan, J. Deisenhofer, and A. Loidl, Phys. Rev. B **83**, 245127 (2011).
  - <sup>21</sup> W. Reiff, I. Grey, A. Fan, Z. Eliezer, and H. Steinfink, Journal of Solid State Chemistry **13**, 32 (1975).